J Mater Sci (2009) 44:3498–3503
DOI 10.1007/s10853-009-3468-x

Characterization of commercial double-walled carbon nanotube material: composition, structure, and heat capacity

Glaura G. Silva · Anthony W. Musumeci · Ana Paula Gomes · Jiang-Wen Liu · Eric R. Waclawik · Graeme A. George · Ray L. Frost · Marcos A. Pimenta

Received: 11 January 2009 / Accepted: 6 April 2009 / Published online: 28 April 2009

Abstract A purified commercial double-walled carbon nanotube (DWCNT) sample was investigated by transmission electron microscopy (TEM), thermogravimetry (TG), and Raman spectroscopy. Moreover, the heat capacity of the DWCNT sample was determined by temperature-modulated differential scanning calorimetry in the range of temperature between −50 and 290 °C. The main thermo-oxidation characterized by TG occurred at 474 °C with the loss of 90 wt% of the sample. Thermo-oxidation of the sample was also investigated by high-resolution TG, which indicated that a fraction rich in carbon nanotube represents more than 80 wt% of the material. Other carbonaceous fractions rich in amorphous coating and graphitic particles were identified by the deconvolution procedure applied to the derivative of TG curve. Complementary structural data were provided by TEM and Raman studies. The information obtained allows the optimization of composites based on this nanomaterial with reliable characteristics.

Introduction

Synthetic methods to prepare relatively pure double-walled carbon nanotubes (DWCNTs) have been developed recently (see for instance references [1–5]). Electronic properties of DWCNTs have been investigated [6–8] and exciting new properties, such as the behavior as cylindrical molecular capacitors [7] and ambipolar transport characteristics [8], were recognized. Tensile strength and Young's modulus of DWCNT strands were found to be comparable to those of single-walled carbon nanotube (SWCNT) bundles [9]. These scientific advances and many others indicate that DWCNTs will briefly be incorporated in several engineering products. Therefore, the time is right to propose a systematic and accessible methodology for DWCNT characterization for applied researchers and engineers [10].

Carbon nanotube commercial materials are characterized by a large distribution of chemical and structural features. This research focuses on the use of thermal methods such as thermogravimetry (TG) and differential scanning calorimetry (DSC) to obtain useful information about this nanomaterial. TG and DSC equipment are readily available in industrial and academic laboratories. Therefore, the data obtained by these techniques could be easily compared for quality control purposes.

Thermo-oxidative stability at temperatures higher than 700 °C has been reported for DWCNTs [3, 11]. The thermal stability behavior depends on the DWCNT matrix purity in relation to metal particles and other carbonaceous contaminants, as well as to variable measurement conditions. It is noted that the diameter distribution, concentration of defects, and interwall interaction can also play an important role in thermo-oxidative stability. Several of these parameters have been reported to be critical in the thermal behavior of SWCNT and multi-walled carbon nanotube (MWCNT) as well [12–14]. Therefore, these aspects will be discussed here as they form an important issue in the carbon nanotube field with a strong impact in large volume applications [10].

G. G. Silva (✉) · A. P. Gomes · M. A. Pimenta
Instituto de Ciências Exatas, Universidade Federal de Minas Gerais, Pampulha, Belo Horizonte, MG 31270-901, Brazil
e-mail: glaura@qui.ufmg.br; glaurasilva@yahoo.com

A. W. Musumeci · J.-W. Liu · E. R. Waclawik · G. A. George · R. L. Frost
School of Physical & Chemical Sciences, Queensland University of Technology, GPO Box 2434, Brisbane, QLD 4001, Australia

Osswald and co-workers [15, 16] performed a detailed investigation of SWCNT and DWCNT oxidation through in situ Raman spectroscopy. A decrease in the D band intensity of DWCNT was shown starting around 370 °C. The authors concluded that an isothermal oxidation can be used as an efficient purification method [16].

Gozzi et al. [17] recently showed a successful strategy to separate mixtures of carbonaceous by sequential removal of carbon in a thermogravimetric experiment under CO_2 stream. The most reliable results were obtained when the carbonaceous sample was mixed with a catalyst, such as Cr_2O_3, to improve the release of CO from the surface.

Thermal expansion coefficient and heat capacity are important thermal parameters from the point of view of fundamental and applied research. Thermal expansion coefficients of SWCNTs and DWCNTs have been found to be quite similar [18]. The interlayer spacing between inner and outer tubes in DWCNTs characterized by Abe et al. [18] was 0.36 ± 0.01 nm. Otherwise, values for the inter-tube spacing ranging from 0.33 to 0.45 nm have been reported for DWCNT samples [19].

The specific heat capacity of carbon nanotubes has been studied both theoretically and experimentally by using different techniques, most in a low temperature range [20–22] with sophisticated apparatus. Purified and crystallized SWCNT ropes were investigated by Hone et al. [23] in the temperature range between 2 and 300 K. At 300 K, the C_p value was approximately 0.65 J g^{-1} K^{-1} and a monotonic decrease of C_p as a function of temperature was observed down to 2 K. In the present work, we attempt to determine the heat capacity of a typical DWCNT sample by using temperature-modulated DSC in the range 223–563 K. This range of temperature (−50 to 290 °C) is a frequent working range for materials such as polymer nanocomposites. The determined C_p values of carbon nanotubes will be useful to design overall materials properties.

Experimental

DWCNT Nanocyl 2100 material was used as-received. The supplier produces this carbonaceous sample by catalytic carbon vapor deposition and claims to purify their product to greater than 90% carbon as determined by TG. The supplier procedure of purification was not disclosed.

The heat capacity was measured between −50 and 290 °C by using temperature-modulated DSC. A Q100 TA Instruments DSC was calibrated with an indium standard for temperature and with a sapphire standard for heat capacity. Cyclic runs between −50 and 290 °C were performed at 5 °C min^{-1} (modulation of ±0.5 °C each 60s) with approximately 3-mg samples placed in aluminum crucibles under nitrogen atmosphere. The results showed a significant dispersion, which may be due to the heterogeneity of the sample and the small mass used for the measurements. Therefore, a large number of measurements were carried out with different samples and the final results were the average of 10 runs for the DWCNT. For comparison, the heat capacity of a SWCNT Nanocyl 1100 sample was also measured. The SWCNT average diameter was 2 nm and the carbon purity greater than 80% as reported by the supplier and confirmed by in-house transmission electron microscopy (TEM) and TG measurements.

Transmission electron microscopy was carried out with a Philips Tecnai F20 (Field emission electron gun) with an acceleration voltage of 200 kV. Samples for TEM studies were prepared by sonicating diluted DWCNT dispersions in chloroform using a low power ultrasonic bath for several hours and drop casting onto a carbon-coated copper grid.

Thermogravimetry was carried out in a TA® Instruments Inc. high-resolution thermogravimetric analyser (series Q500) in a flowing air atmosphere (60 cm^3/min). Approximately 5 mg of fine powder sample was heated in an open platinum crucible up to 1,000 °C with different procedures: (i) conventional TG at rate of 5.0 °C/min performed in triplicate; (ii) high-resolution TG (HRTG) measurement at 10.0 °C/min with resolution 6 and sensitivity 1 (index of the equipment) performed in duplicate. Derivative thermogravimetric (DTG) curves were generated with approximately 2,000 points for the conventional TG and 6,000 points for the HRTG. The data were analyzed by nonlinear least squares fit to multiple Gaussian/Lorentzian or Gaussian curves; the minimum number of curves was used to fit DTG until the adjustment was judged visually satisfactory and correlation coefficient greater than 0.999 was obtained.

The Raman measurements were carried out using a Dilor XY triple-spectrometer equipped with a charge coupled device (CCD) operating at the nitrogen liquid temperature. The lines 457.9, 488, 514.5, 568.2, and 647.1 nm of an Ar–Kr laser were used as the excitation source. The measurements were performed in a backscattering geometry, using an 80× objective lens. The laser power was kept below 1 mW in order to avoid heating effects [24].

Results and discussion

Heat capacity of DWCNT sample

Heat capacity of the DWCNT material was determined by temperature-modulated DSC [25]. The values of heat capacity, shown in Fig. 1, correspond to the "in phase" with the modulation value. A large standard error was assessed by

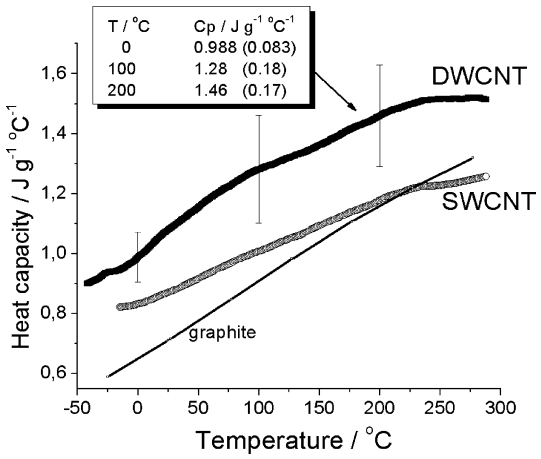

Fig. 1 Heat capacity of DWCNT, SWCNT samples, and graphite [26]. Data for DWCNT at three temperatures and standard error (in *brackets*) are shown in the figure

analyzing 10 heat capacity measurements of DWCNT samples, which was attributed to the small mass (~3 mg) used to perform the experiment and the inhomogeneities of the sample. At 27 °C, Hone et al. [23] determined a C_p value of 0.65 J g^{-1} K^{-1} for purified and crystallized SWCNT ropes under vacuum; the average diameter of these tubes was 1.25 nm. The value obtained at 27 °C for the sample of DWCNTs under N_2 in this work is (1.085 ± 0.089 J g^{-1} $°C^{-1}$), which is significantly higher than the SWCNT and graphite values in the literature [23, 26].

In order to understand the DWCNT C_p result obtained under N_2 atmosphere, a SWCNT sample from the same supplier of the DWCNTs was also characterized. A three times higher amount of nanotubes were loaded in the pan for the SWCNT measurement because the sample was much denser and the standard error (evaluated from triplicate measurements) of the C_p data decreased to less than 2% of the experimental value. The values of C_p obtained for the SWCNT, as shown in Fig. 1, were (in J g^{-1} $°C^{-1}$): 0.832 (0 °C), 0.874 (27 °C), 1.007 (100 °C), and 1.178 (200 °C). These values are smaller than the DWCNT but higher than the values observed by other authors [23]. Linearity of C_p with temperature was observed experimentally from ~50 to 200 K [21] and 300 K [20, 23]. Figure 1 shows the change of slope of the curve close to 483 K (210 °C). The influence of the N_2 adsorbed may be important and variable depending on the temperature and can be the cause of the higher values of heat capacity in relation to other works [21, 23] and to the observed change in slope.

DWCNT characterization by TEM and TG

Typical TEM images of three different regions shown in Fig. 2 show the presence of DWCNTs and SWCNTs in the as-received material. The arrows indicate SWCNTs, while all other bundles and isolated tubes are DWCNTs. Figure 2b only exhibits DWCNTs. An evaluation performed by counting the number of SWCNTs and DWCNTs in typical images (e.g., as shown in Fig. 2) gave an approximate value of 20% SWCNT content in the sample. MWCNTs were not observed in these samples. The diameter distribution for the outer tube of the DWCNTs was evaluated by measuring a few isolated tubes in the TEM images, giving an average value of 2.6 nm. The inner diameter assessment gave an average value of 1.1 nm. The small amount of available TEM images with enough resolution for diameter assessment did not allow a final result for this parameter by microscopy. The length of the DWCNT bundles observed in SEM images (not shown) was found to be greater than 2 μm. TEM images also showed the presence of metal particles encapsulated by carbon multishells and an amorphous carbon coating.

Thermogravimetric measurements for the DWCNT material were performed in triplicate to assure accuracy in relation to possible inhomogeneities of the sample [10]. The typical TG curve at 5 °C min^{-1} and its derivative DTG are shown in Fig. 3. Figure 3b presents the region of the main mass loss peak and line shape analyses performed to fit the DTG curve by Gaussian lines. Table 1 shows the

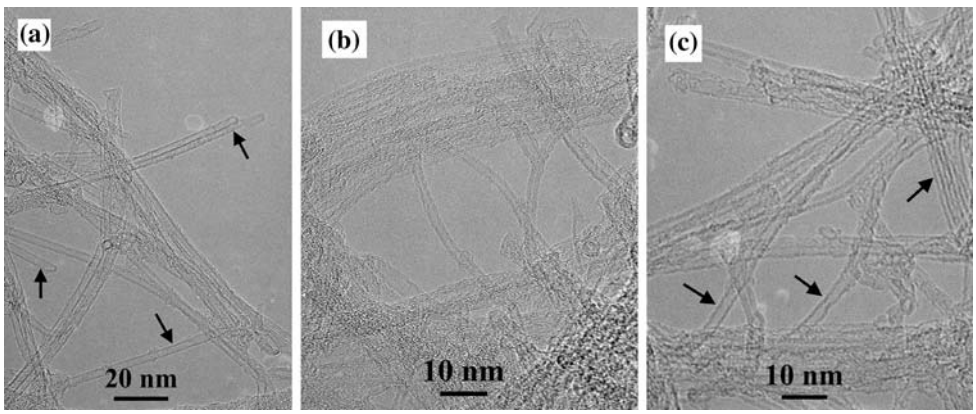

Fig. 2 TEM images of three different regions of the DWCNT. *Arrows* indicate SWCNTs and all other tubes are DWCNTs

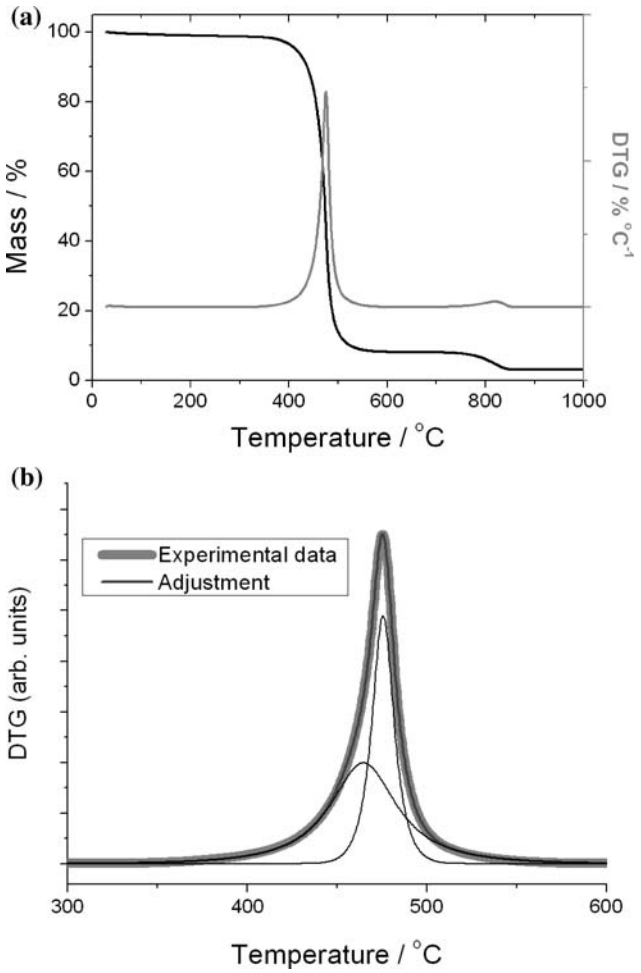

Fig. 3 (**a**) TG and (**b**) DTG curves for DWCNT obtained at 5 °C min^{-1} in air. Line-shape analysis of the main mass loss

Table 1 Thermogravimetric results obtained at 5 °C min^{-1} for DWCNT

TG results		DTG (300–600 °C) line-shape results	
T_d^{max}	Mass loss (%)	First line[a]	Second line
474	90	$T_1 = 465$ °C	$T_2 = 475$ °C
816	5.0	$W_1 = 44$	$W_2 = 14$
Residue: 3.6%		$A_1 = 58\%$	$A_2 = 42\%$

Peak positions and mass loss for the two independent decomposition stages (average of triplicate). Line-shape analyses results for the main thermal oxidation

T_i = position, W_i = full width at half maximum, and A_i = area of the adjustment lines

[a] Lines were composed by Gaussian and Lorentzian contributions

results of this TG experiment and line-shape analysis of the main decomposition.

The main carbonaceous decomposition, shown in Fig. 3 and Table 1, occurs at 474 °C and a second oxidative decomposition was observed at 816 °C, which corresponds to 5 wt% of the sample. The metal oxide residue is only 3.6 wt%, which indicates the good quality of the carbon nanotube purified sample [10] examined in this study as claimed by the supplier. The main oxidation profile was well fitted by two lines corresponding to 58% and 42% relative mass of the material decomposing. Figure 3b shows that the first line is quite broad with a width of 44 °C (Table 1) and it cannot be assigned to a specific type of carbonaceous material [12, 13].

In order to obtain more detailed information about the thermo-oxidation behavior of the carbonaceous sample, a TG experiment was conducted in a HRTG mode. Figure 4 shows the heating protocol applied to the sample and the line-shape analysis of the DTG curve as a function of time. The heating rate is not linear in a HRTG experiment as it depends on the reaction rate and is corrected to allow a controlled reaction rate, which is defined by the resolution set control of the machine, in this case resolution 6. Therefore, during the main decomposition the experiment is quasi-isothermal, as can be observed in Fig. 4a, and a sample with overlapped thermo-oxidation of components may show fractions decomposing at separate times. The

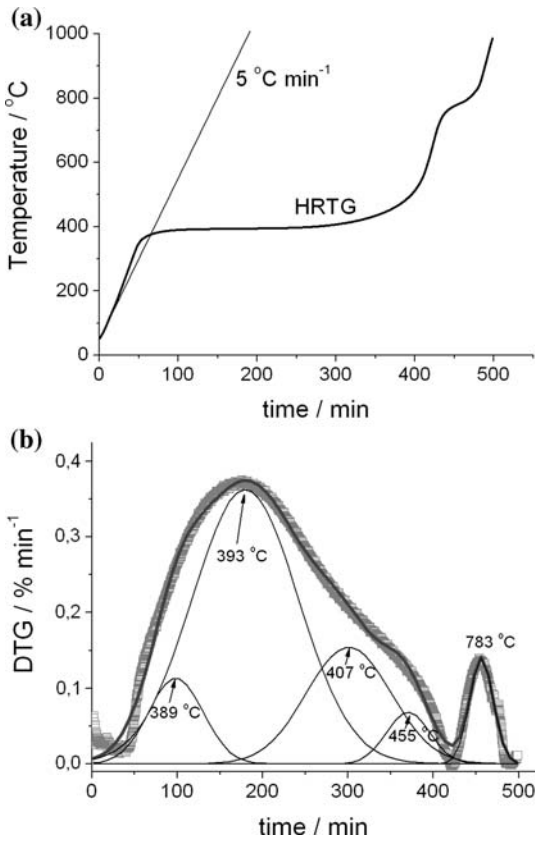

Fig. 4 High-resolution thermogravimetry (HRTG) of DWCNT: (**a**) heating run in the HRTG compared with the linear heating of 5 °C min^{-1} and (**b**) derivative of the HRTG (DTG) curve as a function of time and line-shape results by using Gaussian lines

line-fit analysis, by using pure Gaussian curves in Fig. 4b, allows the determination of four main lines for the thermo-oxidative decomposition of the DWCNT sample. The assignment of these lines to fractions of carbonaceous material can be rationalized based upon SEM and TEM images and also by taking into account the relative reactivity of different carbonaceous materials. For a more complete discussion on this subject please see references [12, 13]. The first line at 389 °C in Fig. 4b corresponds to 9% of the sample and can be assigned to a fraction enriched with amorphous defective coating, which overlaps with the carbon nanotube oxidation. The second and third lines at 393 and 407 °C, respectively, may be considered as carbon nanotube rich fractions with slightly different reactivity. These intermediate fractions correspond to 56% and 19% of the total mass. The fraction oxidizing at 455 °C corresponds to 4% of the sample and was assigned to the decomposition of mainly graphitic shells. Although this attribution is supported by the qualitative evaluation of the TEM images, it is clear that the overlapped lines observed in Fig. 4b do not allow a specific assignment and we only claim that the fractions are enriched in a type of carbonaceous material, in the order amorphous–nanotube–graphitic, as the temperature increases. Gozzi et al. [17] showed a better separation with a procedure in CO_2 atmosphere with the help of catalyst addition to improve CO release.

After the main decomposition at 474 °C, a second oxidation corresponding to 5 wt% of the sample was observed by TG at 816 °C (Fig. 3). This material shows a peak in the DTG curve of the HRTG experiment at 783 °C as can be observed in Fig. 4b. The TEM images for this fraction (not shown) revealed the presence of strands of nanotubes together with a high content of metal oxide particles.

Raman study of DWCNT sample

Raman spectroscopy has been applied for the characterization of DWCNT samples [27, 28]. Five available laser-excitation energies were used to collect Raman spectra of the DWCNT sample in this study. The region of the G band (or tangential mode) for the DWCNTs sample is shown in Fig. 5a. The D band observed in the spectra of Fig. 5 at $\sim$1,340 cm^{-1} is typical of as-grown and moderately purified carbon nanotubes. A quantitative evaluation of the amount of the carbonaceous components is not directly obtained by Raman spectroscopy, in contrast to HRTG measurements, as presented above. For a DWCNT sample, Osswald et al. [16] reported the decrease of the ratio between the D and G bands intensities as a function of time at temperatures between 350 and 550 °C. These authors observed

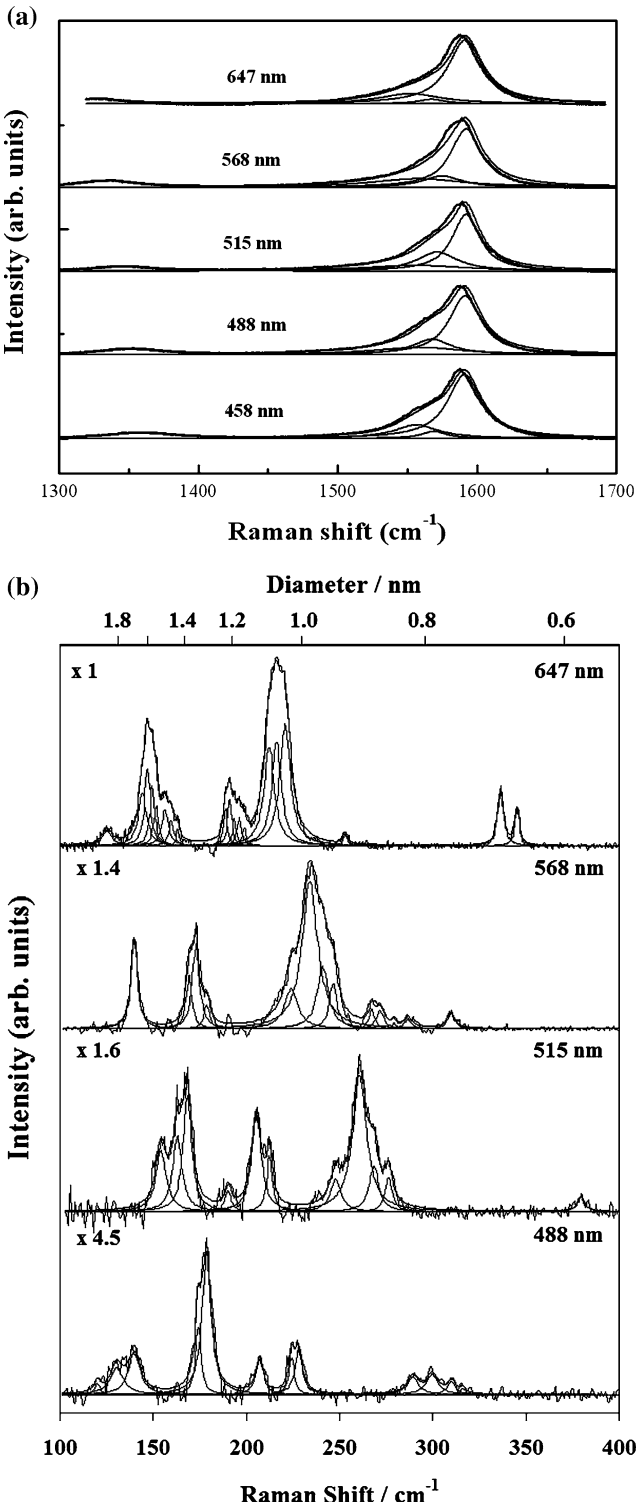

Fig. 5 Raman spectra and Lorentzian line-shape analysis for DWCNT in the region of the G and D bands (**a**) and in the RBM region (**b**). Spectra at specified laser excitation. Diameters on top of the RBM spectra (**b**) were obtained from peak position of Lorentzian lines by using $\omega_{RBM} = [223/d] + 10$ [24]

for the spectra recorded at 633 nm excitation wavelength an I_D/I_G of 0.25; the ratio rapidly decreases in oxidation treatments at temperatures higher than 475 °C. This ratio can be used for comparison strictly between data collected at the same laser excitation energy [29]. However, the value of I_D/I_G for DWCNT equal to 0.15, obtained in the present work for the excitation energy of 647 nm (close to 633 nm), may be considered as an evidence of nanotube quality.

The low wavenumber region in Fig. 5b shows the radial breathing mode (RBM) peaks at four laser excitations. The lower intensity of the signal at 458 nm in this region prevents the analysis of the RBM at this laser energy. The results in Fig. 5b allow an assessment of nanotube diameter by using the equation $\omega_{RBM} = [223/d] + 10$ (ω_{RBM} = RBM frequencies) [24]. Large-diameter nanotubes were not detected in the RBM Raman region. The nanotubes with diameter between 1.3 and 0.8 nm shown in Fig. 5b (see upper scale) are assigned to the inner tubes of DWCNTs or SWCNTs in the sample. The range of outer diameter characterized by Raman (RBM) is limited between 1.4 and 2.0 nm as can be seem in Fig. 5b. TEM images indicated a higher range of values for the outer diameter; however, the number of nanotubes estimated using TEM images was low.

Conclusions

This work provides a detailed characterization of a carbonaceous sample by the interplay of temperature-modulated DSC, HRTG, TEM images, and Raman spectroscopy. The commercial sample is composed of less than 3 wt% metal particles, and close to 80 wt% nanotubes as can be inferred from the HRTG study. The other carbonaceous are amorphous coatings and graphitic particles. Furthermore, TEM images indicated the presence of approximately 20% of SWCNTs within the DWCNT sample. The DWCNT average outer tube diameter was approximately 1.6 nm and the inner tube diameter was 1.0 nm as evaluated by Raman spectroscopy with the analysis of the RBM region.

Heat capacity values for the DWCNT-based sample in the presence of N_2 were characterized as varying between 0.988 J g^{-1} $°C^{-1}$ at 0 °C and 1.46 J g^{-1} $°C^{-1}$ at 200 °C. This value of C_p is characteristic of a sample with the above-mentioned composition and structural characteristics. Therefore, is a useful value in the context of processing and assembling nanomaterials based on this commercial DWCNT.

Acknowledgements G. G. Silva thanks the Brazilian agency CAPES for grant. This work was partially supported by Rede Nacional de Pesquisa em Nanotubos de Carbono/CNPq, Brazil. ERW gratefully acknowledges financial support from the United States Air Force's Asian Office of Aerospace Research and Development. Project ID: AOARD-06-4041.

References

1. Hutchison JL, Kiselev NA, Krinichnaya EP, Krestinin AV, Loutfy RO, Morawsky AP, Muradyan VE, Obraztsova ED, Sloan J, Terekhov SV, Zakharov DN (2001) Carbon 39:761
2. Flahaut E, Bacsa R, Peigney A, Laurent C (2003) Chem Commun 1442
3. Huang HJ, Kajiura H, Tsutsui S, Murakami Y, Ata M (2003) J Phys Chem B 107:8794
4. Endo M, Muramatsu H, Hayashi T, Kim YA, Terrones M, Dresselhaus NS (2005) Nature 433:476
5. Hiraoka T, Yamada T, Hata K, Futaba DN, Kurachi H, Uemura S, Yumura M, Iijima S (2006) JACS 128:13338
6. Kociak M, Suenaga K, Hirahara K, Saito Y, Nakahira T, Iijima S (2002) Phys Rev Lett 89:155501
7. Chen GG, Bandow S, Margine ER, Nisoli C, Kolmogorov AN, Crespi VH, Gupta R, Sumanasekera GU, Iijima S, Eklund PC (2003) Phys Rev Lett 90:257403
8. Shimada T, Sugai T, Ohno Y, Kishimoto S, Mizutani T, Yoshida H, Okazaki T, Shinohara H (2004) App Phys Lett 84:2412
9. Li YJ, Wang KL, Wei JQ, Gu ZY, Wang ZC, Luo JB, Wu DH (2005) Carbon 43:31
10. Arepalli S, Nikolaev P, Gorelik O, Hadjiev VG, Bradlev HA, Holmes W, Files B, Yowell L (2004) Carbon 42:1783
11. Muramatsu H, Hayashi T, Kim YA, Shimamoto D, Kim YJ, Tantrakarn K, Endo M, Terrones M, Dresselhaus MS (2005) Chem Phys Lett 414:444
12. Musumeci AW, Silva GG, Martens WN, Waclawik ER, Frost RL (2007) J Therm Anal Calorim 88:885
13. Trigueiro JPC, Silva GG, Lavall RL, Furtado CA, Oliveira S, Ferlauto AS, Lacerda RG, Ladeira LO, Liu JW, Frost RL, George GA (2007) J Nanosci Nanotechnol 7:3477
14. Zhang XX, Deng CF, Xu R, Wang DZ (2007) J Mater Sci 42:8377. doi:10.1007/s10853-007-1941-y
15. Osswald S, Flahaut E, Ye H, Gogotsi Y (2005) Chem Phys Lett 402:422
16. Osswald S, Flahaut E, Gogotsi Y (2006) Chem Mater 18:1525
17. Gozzi D, Latini A, Lazzarini L (2008) Chem Mater 20:4126
18. Abe M, Kataura H, Kira H, Kodama T, Suzuki S, Achiba Y, Kato K, Takata M, Fujiwara A, Matsuda K, Maniwa Y (2003) Phys Rev B 68:041405
19. Bichoutskaia E, Heggie MI, Popov AM, Lozovik YE (2006) Phys Rev B 73:045435
20. Mizel A, Benedict LX, Cohen ML, Louie SG, Zettl A, Budraa NK, Beyermann WP (1999) Phys Rev B 60:3264
21. Yi W, Lu L, Zhang DL, Pan ZW, Xie SS (1999) Phys Rev B 59:R9015
22. Li CY, Chou TW (2005) Mater Sci Eng A 409:140
23. Hone J, Batlogg B, Benes Z, Johnson AT, Fischer JE (2000) Science 289:1730
24. Fantini C, Jorio A, Souza M, Strano MS, Dresselhaus MS, Pimenta MA (2004) Phys Rev Lett 93:147406
25. Reading M (2001) J Therm Anal Calorim 64:7
26. Dinsdale AT (1991) Calphad 15:317
27. Li F, Chou SG, Ren WC, Gardecki JA, Swan AK, Unlu MS, Goldberg BB, Cheng HM, Dresselhaus MS (2003) J Mater Res 18:1251
28. Kim YA, Muramatsu H, Kojima M, Hayashi T, Endo M, Terrones M, Dresselhaus MS (2006) Chem Phys Lett 420:377
29. Cancado LG, Takai K, Enoki T, Endo M, Kim YA, Mizusaki H, Jorio A, Coelho LN, Magalhaes-Paniago R, Pimenta MA (2006) App Phys Lett 88:163106